Journal of Engg. Research Vol. 7 No. (4) December 2019 pp. 18-36

Seismic analysis of shallow tunnel collapse mechanisms with the horizontal slice method

Guo Zi-hong*, Liu Xin-rong**, Li Lin* and Zhu Zhanyuan***

**College of Civil Engineering, Sichuan Agricultural University, Sichuan, Dujiangyan 611830, China*
***College of Civil Engineering, Chongqing University, Chongqing 400045, China*
****Sichuan Higher Institution Engineering Research Center of Rural Construction Disaster Prevention and Reduction, Dujiangyan 611830, China*
**Corresponding Author: guozihonghyx@sicau.edu.cn*

ABSTRACT

The paper presents an analytical method to evaluate tunnel collapse mechanisms during earthquakes; seismic solutions are established based on the horizontal slice method and the variational principle. Different sliding surfaces are applied to be compared with each other, and the finite difference method is employed to verify the analytical results. Then, the conclusions come out that it is conservative to leave out the vertical force and regard the static earth pressure as the horizontal stress at the vault section. Curved sliding surfaces are more reasonable than the linear sliding surface. The tunnel safety factors on a sliding surface change between 0.89 and 2.44 during earthquakes with 0.3g. When the number of undetermined constants is 2 and the different locations of the start damage point are taken into account, the curved sliding surface is reasonable to analyze the shallow tunnel collapse mechanisms, and the analytical results have excellent agreement with the numerical simulation and previous studies. By parameter analysis, it shows that the tunnel depth & radius, friction angle, and cohesion of soil have an obvious influence on the sliding surface distribution. Tunnel radius and cohesion of surrounding soil are the two most important factors influencing the tunnel stability. Reducing the tunnel radius and increasing cohesion are the most useful ways to enhance shallow tunnel stability during earthquakes.

Keywords: Seismic analysis; shallow tunnel; collapse mechanisms; horizontal slice method; variational principle.

INTRODUCTION

In the process of infrastructure construction, tunnels serve as a popular method to take advantage of underground space and are regarded as aseismic structures during earthquakes. However, tunnels have been demonstrated to be vulnerable to seismic damage if tunnel depth is shallow or faults exist, as shown in the latest Chi-Chi Earthquake (Wang et al., 2001), Wenchuan Earthquake (Wang & Zhang, 2013) and so on. Many researchers have focused on tunnel seismic analysis. The isolation mechanism of tunnels was studied with dynamic centrifuge tests (Chen & Shen, 2014). Utility tunnels under non-uniform earthquake excitation were analyzed with numerical simulations (Chen et al., 2012) and a theoretical method was presented to analyze the dynamic response of a circular lined tunnel subjected to plane P-waves (Yi et al., 2016).

Shallow tunnels are very susceptible to earthquake damage in alluvial deposits (Argyroudis & Pitilakis, 2012). Numerical simulation has been applied to assess the effect of liquefaction on shallow shield tunnels (Azadi & Mir Mohammad Hosseini, 2010) and to analyze the dynamic behavior of shallow circular tunnels in two different clayey deposits (Amorosi & Boldini, 2009; Gomes et al., 2015). Model tests have been built to analyze the dynamic response of a portal section of a mountain tunnel (Tao et al., 2015). In addition to those methods, the limit equilibrium method has been widely applied to studied shallow tunnel stability because it is practicable for engineers. The load for a shallow tunnel support structure can be evaluated using the Terzaghi failure mode, and Lei et al. used this method to

analyze the surrounding rock pressure using nonlinear failure criteria and a linear sliding surface (Lei et al., 2014). Based on the broken line sliding surface, the upper and lower bound stability solutions have been derived for collapse under undrained conditions (Davis et al., 1980), and the safety factor for shallow tunnels in saturated soil has been calculated using the strength reduction technique (Yang & Huang, 2009). Using the curved sliding surface, an exact solution for the collapse mechanisms in cavities and in tunnels according to the Hoek–Brown failure criterion was presented (Fraldi & Guarracino, 2009), and a numerical solution for the shape of the collapsing block in a circular tunnel was derived (Huang & Yang, 2011). The numerical simulations and model test were applied to analyze the sliding surface for a shallow tunnel (Lei et al., 2015; Sterpi & Cividini, 2004; Yamamoto et al., 2011). However, it is still difficult to accurately show a shallow tunnel's sliding surface.

The stability of a circular tunnel in the presence of pseudostatic seismic body forces was studied using an upper bound finite element limit analysis in combination with a linear optimization technique (Sahoo & Kumar, 2014). The influences on the acceleration variation for shallow tunnels were analyzed (Amorosi & Boldini, 2009; Huang et al., 2012). The hypothesis that the horizontal and vertical accelerations are related with depth and time is applied to analyze the seismic designs of retaining wall (Ghosh, 2010; Kolathayar & Ghosh, 2009; Munwar Basha & Sivakumar Babu, 2010). Whether it is proper to apply these relationships to analyze shallow tunnel stability is worth studying.

Shallow tunnel's seismic stability analysis method and collapse mechanism are unsolved issues. However, they are very important to infrastructure construction of the world. To analyze shallow tunnel stability and sliding surface distribution during an earthquake, seismic solutions for shallow tunnel collapse mechanisms are presented using the horizontal slice method and the variation principle. The analytical solutions are compared with the finite difference method. The influences of the main parameters on shallow tunnel stability and sliding surface distribution are analyzed, and methods useful to enhance shallow tunnel stability are proposed.

ANALYSIS MODEL OF SHALLOW TUNNEL

A shallow tunnel during an earthquake is shown in Figure 1, where r is the tunnel radius; q is the supporting pressure, q' is the surface load, h_1 is the shallow tunnel depth, γ is unit weight of soil, F_h and F_v are the horizontal and vertical forces at the vault section AB, which are equal to the integral of the normal and shear stress at the vault section AB, respectively, and H is the vertical distance from the ground surface to the tunnel bottom. The area $A_{CDD'C'}$ is regarded as the roof collapse region, the coordinate of the start point C is (x_0, y_0), and the coordinate of the end point D is (x_1, y_1) at a sliding surface.

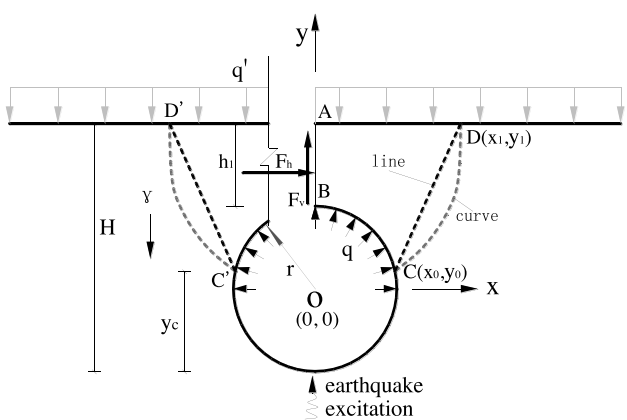

Fig. 1. Shallow tunnel model.

The stress, displacement, and acceleration around a tunnel will change accordingly when the tunnel is subjected to an earthquake. Sahoo et al. established the relationship of the horizontal earthquake acceleration coefficient with other parameters (Sahoo & Kumar, 2014), and the horizontal acceleration obviously increases near the tunnel (Pitilakis et

al., 2014). A reasonable and simple equation to describe the acceleration variation in a field is useful to tunnel stability analysis. Steedman et al. analyzed the seismic characteristics of retailing wall with the assumption that only the phase of acceleration is varying (Steedman & Zeng, 1990). And then the seismic designs of a retaining wall have been analyzed with the acceleration equations that the horizontal and vertical accelerations are related to the depth and time (Ghosh, 2010; Kolathayar & Ghosh, 2009; Basha & Babu, 2010). The equations have the following characters. Firstly, the maximum acceleration decreases with the ground depth and it is consistent with tunnel seismic analysis (Amorosi & Boldini, 2009; Bilotta et al., 2007). Secondly, the direction of acceleration is uniform at the same time in a field, and it is applied to the pseudostatic analysis of tunnel stability (Saada, Maghous, & Garnier, 2013; Sahoo & Kumar, 2014). Thirdly, the phase of acceleration can vary with time and it is useful to analyze tunnel stability with time. The seismic acceleration coefficients are expressed as (Kolathayar & Ghosh, 2009;).

$$k_h = k_{h0}\left[1+(f_a-1)(y+r)/H\right]\sin\omega\left[t-(y+r)/V_s\right] \quad (1)$$

$$k_v = k_{v0}\left[1+(f_a-1)(y+r)/H\right]\sin\omega\left[t-(y+r)/V_p\right] \quad (2)$$

where k_h and k_v are the horizontal and vertical seismic acceleration coefficients at the depth $H-y-r$ and time t in these equations, k_{h0} and k_{v0} are the amplitudes of horizontal and vertical seismic acceleration coefficients at the tunnel bottom, f_a is the acceleration amplification factor at the ground surface, ω is the angular frequency to earthquake excitation, y is the distribution function of the sliding surface, and V_s and V_p are the shear wave velocity and primary wave velocity respectively. k_h and k_v reach the maximum almost at the same time in the case of $V_s >> H$ and $V_p >> H$. Therefore, it is conservative and reasonable to analyze shallow tunnel stability on the hypothesis k_h and k_v reach the extreme simultaneously.

Prior to excavation, the stress distribution in the ground is earth stress at rest. The Jaky equation defines the relationship between the stress coefficient and the inner friction angle (Jaky, 1944), $k_0 = 1-\sin\phi$. According to elastic theory, the stress coefficient can be defined as $k_0 = \nu/(1-\nu)$ for plane strain as well, where ν is Poisson's ratio. Therefore, both methods can be used to calculate the earth stress at rest. When a tunnel is built in the ground, the stress around the tunnel will change. F_v equals zero with $k_h = 0$ because of the symmetry of the load and structure. F_h is not zero and directs upward when the horizontal acceleration is directed toward the left.

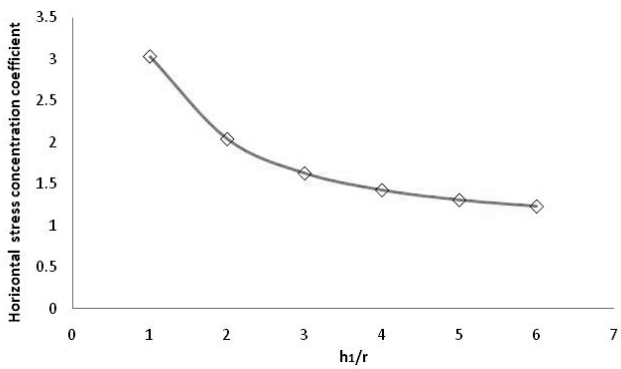

Fig. 2. Variation of the horizontal stress concentration coefficient.

When the surrounding soil is assumed to be an elastic material and the horizontal stress coefficient is defined as the ratio of the mean stress after excavation to the mean initial stress at section AB. 6 shallow tunnel models with different depth are established with FLAC^{3D} without seismic excitation, and then the variation of horizontal stress concentration coefficient at section AB at different tunnel depths without seismic effect is shown in Figure 2. This indicates that the excavation of the tunnel leads to an increase in the horizontal stress at section AB. The horizontal stress concentration

coefficient is 3.03 when h_1/r =1, and the value decreases to 1.23 when h_1/r =6. It is clear that the excavation leads to a stress concentration at section AB. Therefore, the stress at section AB is greater than the earth pressure at rest. However, it cannot exceed the passive earth pressure.

SEISMIC ANALYSIS FOR A SHALLOW TUNNEL

Linear sliding surface

The linear sliding surface is applied to analyze the surrounding soil pressure around a shallow tunnel (Lei et al., 2014). Based on the hypothesis that sliding surface is a line, the shallow tunnel's safety factor, k_{sl}, can be defined as the ratio of the shear resistance to the shear force alone a sliding surface and can be written as

$$k_{sl}=\frac{cl+f\cos\alpha\left[W(1+k_v)+F_h\tan\alpha-F_v-qx_0+q(r-\sqrt{r^2-x_0^2})\tan\alpha-Q\tan\alpha+q'x_1\right]}{W(1+k_v)\sin\alpha+Q\cos\alpha-F_h\cos\alpha-F_v\sin\alpha-q(r-\sqrt{r^2-x_0^2})\cos\alpha-qx_0\sin\alpha+q'x_1\sin\alpha} \tag{3}$$

$$cl=c(H-h-\sqrt{r^2-x_0})\sqrt{1+k^2}\Big/k \tag{4}$$

$$\cos\alpha=1\Big/\sqrt{1+k^2} \tag{5}$$

$$\sin\alpha=k\Big/\sqrt{1+k^2} \tag{6}$$

$$x=\left(y-\sqrt{r^2-x_0^2}\right)\Big/k+x_0 \tag{7}$$

$$W(1+k_v)=\int_{\sqrt{r^2-x_0^2}}^{r}\left[x-\sqrt{r^2-y^2}\right]\gamma(1+k_v)dy+\int_r^{H-h}x\gamma(1+k_v)dy \tag{8}$$

$$Q=\int_{\sqrt{r^2-x_0^2}}^{r}\left[x-\sqrt{r^2-y^2}\right]\gamma k_h dy+\int_r^{H-h}x\gamma k_h dy \tag{9}$$

In equations (3)-(9), k is the slope of the sliding surface, c and f are the cohesion and friction coefficient of the soil, respectively, k_v and k_h are the vertical and horizontal accelerations coefficients during an earthquake, W is the weight of segment A_{ABCD}, and Q is the horizontal body force on A_{ABCD} induced by the earthquake. To solve the extremum problem, k_{sl} must satisfy the following requirements, and the results can be solved using numerical method.

$$\frac{\partial k_{sl}}{\partial x_0}=0,\ \frac{\partial k_{sl}}{\partial k}=0 \tag{10}$$

Curved sliding surface

Upper-bound rigid-block mechanisms have been developed to predict the shallow tunnel's collapse using a polygon, and the simulations determine the collapse along a curve (Yamamoto et al., 2011). Experimental analysis showed that the sliding surface is curve (Lei et al., 2015). A curved failure mechanism was employed to analyze the collapse shape of a shallow tunnel within the framework of the upper bound theorem (F Huang & Yang, 2011). However, how to define a shallow tunnel's sliding surface there is still unsolved. Therefore, the curved sliding surface was applied to analyze a shallow tunnel's stability on the basis of the variational principle. It satisfies different shapes of sliding surface. A small horizontal slice in A_{ABCD} is taken from Figure 1 and is shown in Figure 3.

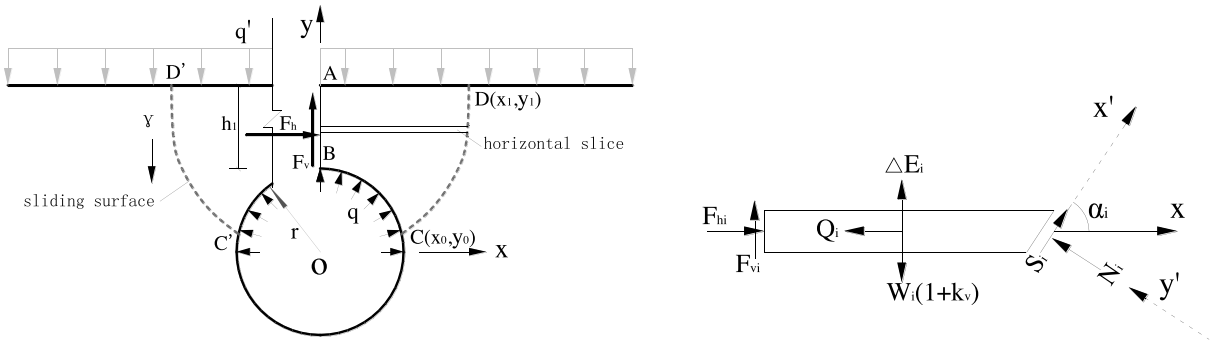

Fig. 3. A horizontal slice of shallow tunnel.

To balance the forces in the x'-direction, the equation can be written as

$$\sum F_{x'} = 0, \quad S_i = Q_i \cos\alpha_i - \Delta E_i \sin\alpha_i + W_i\left(1+k_v\right)\sin\alpha_i - F_{hi}\cos\alpha_i - F_{vi}\sin\alpha_i = \left(c_i l_i + N_i f_i\right)/k_{sc} \tag{11}$$

where S_i is the shear resistance and N_i is the normal force on the small sliding surface, α_i is the angle between the x'-axis and the x-axis, and ΔE_i is the force resultant of the slice's top and bottom. F_{hi} and F_{vi} are the vertical and horizontal forces at section AB during earthquake, W_i is the weight of the slice, Q_i is the horizontal body force of the slice induced by earthquake, l_i is the length of sliding surface in a horizontal slice, and c_i and f_i are the cohesion and friction coefficient of soil. Equation (11) can be rewritten as

$$\Delta E_i = W_i\left(1+k_v\right) + Q_i\cot\alpha_i - F_{hi}\cot\alpha_i - F_{vi} - \left(c_i l_i + N_i f_i\right)\csc\alpha_i / k_{sc} \tag{12}$$

The resultant of all ΔE_i should equal the sum of the surface load and the supporting force in the Y-direction.

$$\sum_1^n W_i\left(1+k_v\right) + \sum_1^n Q_i\cot\alpha_i - \sum_1^n F_{hi}\cot\alpha_i - \sum_1^n F_{vi} - \sum_1^n \left(c_i l_i + N_i f_i\right)\csc\alpha_i / k_{sc} = qx_0 - q'x_1 \tag{13}$$

Then, the shallow tunnel's safety factor k_{sc} for curved sliding surface can be written as

$$k_{sc} = \frac{\sum_1^n \csc\alpha_i\left(c_i l_i + N_i f_i\right)}{\sum_1^n W_i\left(1+k_v\right) + \sum_1^n Q_i\cot\alpha_i - \sum_1^n F_{hi}\cot\alpha_i - F_v - qx_0 + q'x_1} \tag{14}$$

The forces should be balanced in the y'-axis direction and the equation is derived as

$$\begin{aligned} &\sum y' = 0, \quad N_i = W_i\left(1+k_v\right)\cos\alpha_i - \Delta E_i\cos\alpha_i - Q_i\sin\alpha_i + F_{hi}\sin\alpha_i - F_{vi}\cos\alpha_i \\ &\qquad \csc\alpha_i N_i = W_i\left(1+k_v\right)\cot\alpha_i - \Delta E_i\cot\alpha_i - Q_i + F_{hi} - F_{vi}\cot\alpha_i \end{aligned} \tag{15}$$

$$\sum_1^n \csc\alpha_i N_i = \sum_1^n W_i\left(1+k_v\right)\cot\alpha_i - \sum_1^n Q_i + F_h - \sum_1^n \Delta E_i\cot\alpha_i - \sum_1^n F_{vi}\cot\alpha_i \tag{16}$$

The sum of all $\Delta E_i\cot\alpha_i$ is defined as $(qx_0 - q'x_1)\cot\alpha$ because the sum of all ΔE_i equals $qx_0 - q'x_1$, where α is the angle of l_{CD} with x-axis, close to the average value of α_i for a curved sliding surface. Then, this is rewritten as

$$\sum_1^n \csc\alpha N_i = \sum_1^n W_i\left(1+k_v\right)\cot\alpha - \sum_1^n Q_i + F_h - \sum_1^n F_{vi}\cot\alpha_i + \left(q_1x_1 - qx_0\right)\cot\alpha$$
$$\cot\alpha = \left(x_1 - x_0\right)\Big/\left(H - h - \sqrt{r^2 - x_0^2}\right) \tag{17}$$

F_{hi} and F_{vi} are along the vault section AB; therefore the following equations are defined to establish a continuous function $x\left(y\right)$ for the sliding surface.

$$\sum_1^n F_{vi}\cot\alpha_i = F_v\cot\alpha$$
$$\sum_1^n F_{hi}\cot\alpha_i = F_h\cot\alpha \tag{18}$$

Then Equation (14) is rewritten as

$$k_{sc} = \frac{\sum_1^n c_i l_i \csc\alpha_i + f_i\left[\sum_1^n W_i\left(1+k_v\right)\cot\alpha_i - \sum_1^n Q_i + F_h - F_v\cot\alpha + \left(q_1x_1 - qx_0\right)\cot\alpha\right]}{\sum_1^n W_i\left(1+k_v\right) + \sum_1^n Q_i\cot\alpha_i - F_h\cot\alpha - F_v - qx_0 + q'x_1} \tag{19}$$

where the second part of numerator is the friction force, and it should be positive because the direction of the friction force is opposite to the direction of the soil's movement. Point C is regarded as the origin point, and then each part of Equation (19) can be written as

$$\sum_1^n c_i l_i \csc\alpha = \int_0^{H-y_c} c\left(1+x'^2\right)dy \tag{20}$$

$$\sum_1^n W_i\left(1+k_v\right)\cot\alpha_i = \int_0^{2r-y_c}\left[x + x_0 - \sqrt{r^2 - y_c^{\,2}}\right]\gamma\left(1+k_v\right)x'dy + \int_{2r-y_c}^{H-y_c}\left(x+x_0\right)\gamma\left(1+k_v\right)x'dy \tag{21}$$

$$\sum_1^n Q_i = \int_0^{2r-y_c}\left[x + x_0 - \sqrt{r^2 - y_c^{\,2}}\right]\gamma k_h dy + \int_{2r-y_c}^{H-y_c}\left(x+x_0\right)\gamma k_h dy \tag{22}$$

$$\sum_1^n W_i\left(1+k_v\right) = \int_0^{2r-y_c}\left[x + x_0 - \sqrt{r^2 - y_c^{\,2}}\right]\gamma(1+k_v)dy + \int_{2r-y_c}^{H-y_c}\left(x+x_0\right)\gamma(1+k_v)dy \tag{23}$$

$$\sum_1^n Q_i\cot\alpha_i = \int_0^{2r-y_c}\left[x + x_0 - \sqrt{r^2 - y_c^{\,2}}\right]\gamma k_h x'dy + \int_{2r-y_c}^{H-y_c}\left(x+x_0\right)\gamma k_h x'dy \tag{24}$$

$$y_c = r + \sqrt{r^2 - x_0^{\,2}} \tag{25}$$

where x' is the derivative of x.

The horizontal and vertical seismic acceleration coefficients can be rewritten as

$$k_h = k_{h0}\left[1 + (f_a - 1)\left(y + y_c\right)/H\right]\sin\omega\left[t - \left(y + y_c\right)/V_s\right] \tag{26}$$

$$k_v = k_{v0}\left[1 + (f_a - 1)\left(y + y_c\right)/H\right]\sin\omega\left[t - \left(y + y_c\right)/V_p\right] \tag{27}$$

Therefore, the shallow tunnel safety factor can be regarded as the functional $k_{sc}(x, y)$, and its boundary conditions can be written as

$$x_{y=0}=0, \quad x_{y=H-y_c}=x_1-x_0 \tag{28}$$

To attain a homogeneous boundary relating x & y, the function z is defined as

$$z=y-x\left(H-y_c\right)/\left(x_1-x_0\right) \tag{29}$$

Then, the following relationships are derived as

$$x=\left(x_1-x_0\right)\left(y-z\right)/\left(H-y_c\right) \tag{30}$$

$$z_{y=0}=0, \quad z_{y=H-y_c}=0 \tag{31}$$

Equation (28) is the boundary condition for Equations (19) and (29). According to the Ritz method, the basis function $z_n(y)$ can be defined as

$$z_n(y)=\sum_{k=1}^{n} a_n y^n\left(y-H+y_c\right) \tag{32}$$

where a_n is an undetermined constant. Equation (19) combines with Equations (30) and (32) and then, the following equations should be satisfied to solve the minimum value for k_{sc}.

$$\frac{\partial k_{sc}}{\partial x_0}=0, \ \frac{\partial k_{sc}}{\partial x_1}=0 \tag{33}$$

$$\frac{\partial k_{sc}}{\partial a_1}=0, \frac{\partial k_{sc}}{\partial a_2}=0, \ldots, \frac{\partial k_{sc}}{\partial a_n}=0 \tag{34}$$

The issues concerning the sliding surface distribution and safety factor can be solved in light of Equations (33) and (34). The number of the undetermined constants should be selected properly to save calculating time and ensure analysis accuracy. There are many factors that influence the sliding surface distribution and safety factor. The following section will discuss them in detail with the numerical method.

DISCUSSION

Forces at vault

Construction of a tunnel will lead to a stress concentration around the tunnel, and the stress concentration coefficient is more than 1 at section AB in Figure 2. The horizontal acceleration makes the vertical force F_v appear at section AB. An example is taken to analyze the influence of F_h and F_v on the shallow tunnel's safety factor and the sliding surface distribution on the condition that stress coefficient k_0 equals $\nu/(1-\nu)$.

A shallow tunnel is constructed in the ground where γ=20 kN/m^3, α=35°, c=150 kPa, q'=50 kPa, q=20 kPa, k_{h0} = 0.3, k_{v0} = 0.3, f_a = 1.3 , r=6 m, h_1=6 m, H=18 m, $\nu=0.3$, and F_0=218 kN (the integral of earth pressure at rest at section AB). Taking no vertical force F_v into account, the linear and curved sliding surface with 2 undetermined constants (n=2) were applied to analyze the horizontal force's influence on the safety factor and sliding surface, and the results are shown in Table 1. When the horizontal force F_h increases from F_0 to 2.2 F_0, the safety factors increase from 0.894 to 1.030 at the curved sliding surface, and from 1.067 to 1.242 at the linear sliding surface. The safety factor at the curved sliding surface is smaller than that at the linear sliding surface, and the horizontal force F_h has an obvious influence on the safety factor. All the start points are very close to 6 m and end points change from 9.215 m

to 9.304 m at the curved sliding surface. The start and end points of the linear sliding surface change from 5.885 m and 9.125 m to 5.979 m and 9.784 m. The horizontal force F_h has a slight influence on coefficients a_1, a_2 and the slope k, but it has a significant influence on the shallow tunnel stability. The roof collapse area decreases slightly with an increase in the horizontal force.

Table 1. Horizontal force influence on the safety factor and the sliding surface.

F_h/F_0		1	1.2	1.4	1.6	1.8	2	2.2
curved sliding surface	k_{sc}	0.894	0.916	0.938	0.960	0.983	1.007	1.030
	x_0/m	6.000	6.000	6.000	6.000	6.000	6.000	6.000
	x_1/m	10.068	10.105	10.149	10.179	10.204	10.253	10.286
	a_1	0.173	0.174	0.173	0.174	0.175	0.173	0.171
	a_2	-0.008	-0.008	-0.007	-0.008	-0.008	-0.007	-0.007
linear sliding surface	k_{sl}	1.067	1.095	1.124	1.153	1.182	1.212	1.242
	x_0/m	5.885	5.908	5.928	5.944	5.958	5.970	5.979
	x_1/m	9.125	9.247	9.364	9.476	9.583	9.686	9.784
	k	3.342	3.280	3.221	3.167	3.115	3.067	3.022

Table 2. The vertical force's influence on the safety factor and sliding surface.

F_v/F_h		0	0.1	0.2	0.3	0.4	0.5	0.6
curved sliding surface	k_{sc}	0.894	0.901	0.908	0.916	0.923	0.931	0.938
	x_0/m	6.000	6.000	6.000	6.000	6.000	6.000	6.000
	x_1/m	10.068	10.125	10.189	10.260	10.308	10.377	10.461
	a_1	0.173	0.174	0.173	0.171	0.173	0.172	0.168
	a_2	-0.008	-0.008	-0.008	-0.007	-0.008	-0.007	-0.007
linear sliding surface	k_{sl}	1.067	1.079	1.091	1.102	1.114	1.126	1.138
	x_0/m	5.885	5.902	5.918	5.932	5.945	5.956	5.966
	x_1/m	9.125	9.303	9.481	9.659	9.838	10.017	10.196
	k	3.342	3.212	3.091	2.979	2.874	2.778	2.687

When the parameters are fixed with $F_h=F_0$, the vertical force influence on the safety factor and sliding surface is shown in Table 2. When the vertical force increases from zero to 0.6 F_h, k_{sc}, x_1, a_1 and a_2 change from 0.874, 9.215 m, 0.240 and -0.002 to 0.922, 9.708 m, 0.215 and -0.002 at the curved sliding surface, respectively, and k_{sl}, x_0, x_1 and k change from 1.067, 5.885 m, 9.125 m and 3.342 to 1.138, 5.966 m, 10.196 m and 2.687 at linear sliding surface, respectively. This shows that the vertical force's influence on safety factor and the roof collapse area is very slight, and the safety factor at the curved sliding surface is smaller than that at the linear sliding surface.

The finite difference method (FLAC^{3D}) was applied to analyze the shallow tunnel's stability and to compare with the analytical methods. The numerical model of shallow tunnel is shown in Figure 4, the parameters being consistent with the previous example. The surrounding rock is regarded as a Mohr-Coulomb material, the left and right boundaries are fixed in the X-direction displacement, the bottom boundary is fixed in the Z-direction displacement, the front and behind boundaries are fixed in the Y-direction displacement, the surface load and supporting pressure can be applied at the ground surface and tunnel boundary, respectively, the pseudo-static seismic acceleration is employed to analyze shallow tunnel (Sahoo & Kumar, 2014), and it is compatible with Equations (1) and (2).

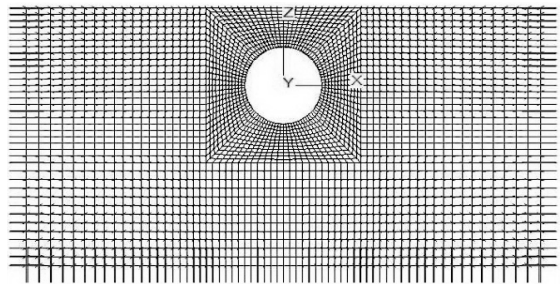

Fig. 4. Numerical model of shallow tunnel.

To analyze the influence of F_h on tunnel safety factor, F_h is regarded as F_0 (the integral of earth pressure at rest) and F_P (the integral of the passive earth pressure), respectively, $f_a = 1.0$, $F_v = 0$, and the numerical simulation is employed to compare with them. A comparison of safety factor using different accelerations is shown in Figure 5. All the data show that an increase in the acceleration coefficients reduces the tunnel safety factors, and their trends are similar to each other. The safety factors with the linear sliding surface are greater than those with the curved sliding surface. The safety factors with the numerical simulation are greater than those with F_0, smaller than with F_P.

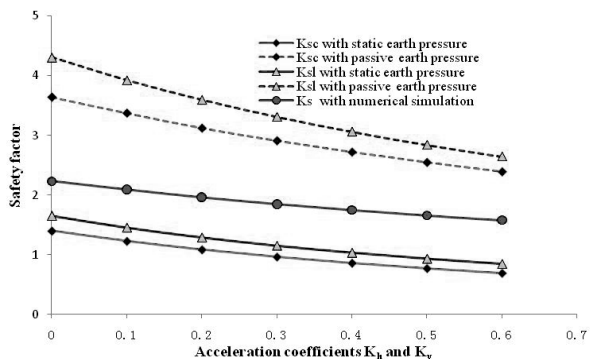

Fig. 5. Comparison of safety factor for different acceleration coefficients.

When $f_a = 1.0$, $a_h = 0.3$ and other parameters are fixed, a comparison of safety factor using different tunnel depths is shown in Figure 6. The safety factors from the numerical simulation are smaller than when using the passive earth pressure and are greater when using with earth pressure at rest. If F_h is defined as F_0, the safety factor continues to decrease with an increase in the tunnel depth. If F_h is defined as F_p, an increase in the tunnel depth enhances the safety factors in the case of the linear sliding surface, but reduces the safety factors in the case of the curved sliding surface. The simulation shows that an increase in the tunnel depth reduces the safety factor very slowly.

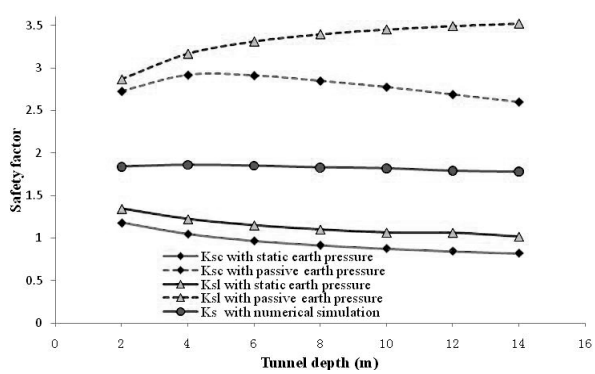

Fig. 6. Comparison of safety factor for different tunnel depths.

Because both the vertical force F_v and horizontal force F_h are advantageous to the tunnel stability and it is difficult to accurately calculate their value under different conditions, it is conservative and reasonable to leave out F_v and to assume F_h as F_0. The following analyses were performed accordingly.

Sliding surface distribution

A reasonable sliding surface will allow us to determine where the most dangerous region is located and to determine the credible safety factor for shallow tunnels. To analyze the difference of sliding surfaces, the stabilities for shallow tunnels were studied using the linear and the curved (n=1~4, the number of undetermined constant a_n) sliding surfaces. According to Equations (25) and (26), k_h and k_v belong to the regions of $(-k_{h0} \sim k_{h0})$ and $(-k_{v0} \sim k_{v0})$ after one earthquake excitation. The time of one excitation is divided into 12 parts to analyze the variations in the shallow tunnel's safety and sliding surface.

Based on the previous example, the relationship of the safety factors with time is shown in Figure 7. The trends in the safety factor for different sliding surfaces are similar to each other. The safety factors vary greatly with time. The largest and smallest safety factors were 2.44 and 0.89 at the curved sliding surface with n=2 in an excitation of earthquake. Therefore, the stress at a sliding surface during an earthquake is a variable, not a constant. The safety factors with the linear sliding surface were larger than those with the curved sliding surface. The safety factors with n=1 have the largest value in the four curved sliding surfaces. But their differences are small. K_1 represents the difference of safety factor between the curved sliding surface (n=2) and the linear sliding surface. The smallest difference was 0.17, which appeared at the smallest safety factor, and the largest difference of 0.43 appeared at the largest safety factor. It is clear that seismic analysis using the linear sliding surface will overestimate tunnel stability.

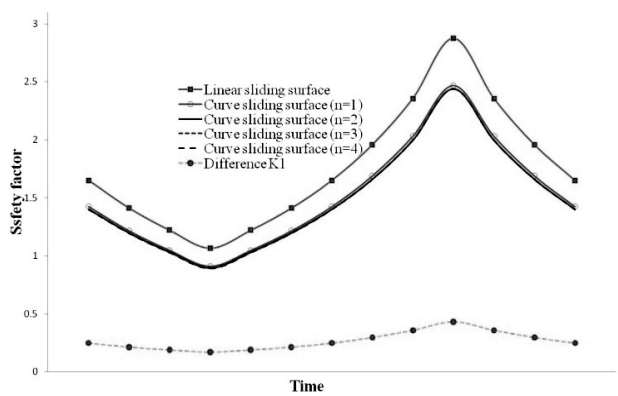

Fig. 7. The relationship of the safety factors with time.

The linear sliding surface is compared with the curved sliding surfaces with n=1~4, and the results from the sliding surfaces over one earthquake excitation are shown in Figure 8. The differences between the curved and linear sliding surfaces are obvious. The curved sliding surfaces with n=2~4 are close to each other and have a little difference from the sliding surface with n=1.

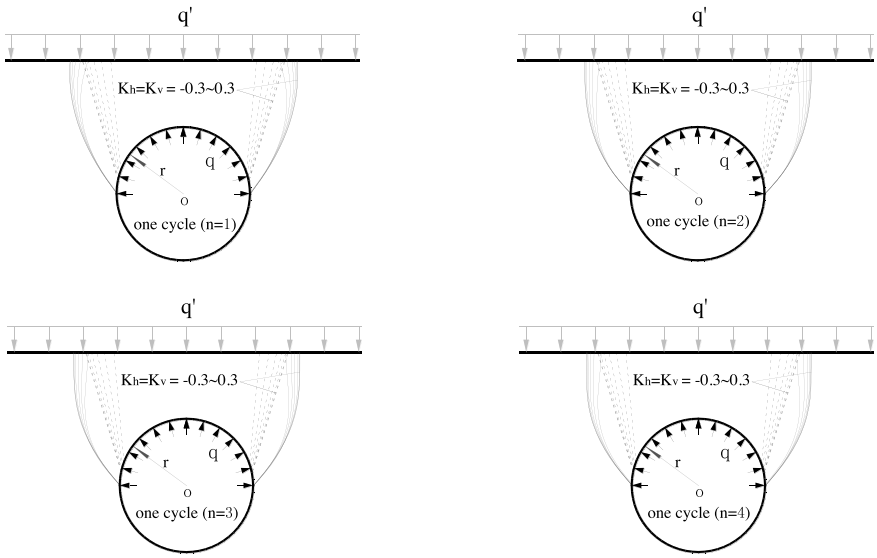

Fig. 8. Comparison of the sliding surfaces over one earthquake excitation.

When h_1=12 m and $k_h = k_v = 0$, the shear-strain increment of the FLAC^{3D} is shown in Figure 9 (a) based on the strength reduction method (Huang, Zhang, Sun, & Jin, 2012). The potential yield fields are consistent with the previous studies on shallow tunnel collapse mechanisms (Sterpi & Cividini, 2004; Yamamoto et al., 2011), as shown in Figures 9 (b) and (c). All the potential yield fields show good agreement with the curved sliding surfaces in Figure 8, and these collapse areas are consistent with the experimental results (Lei et al., 2015). However, the location of start point C possibly appears below hance according to these studies. How to accurately decide the location of point C is another important issue.

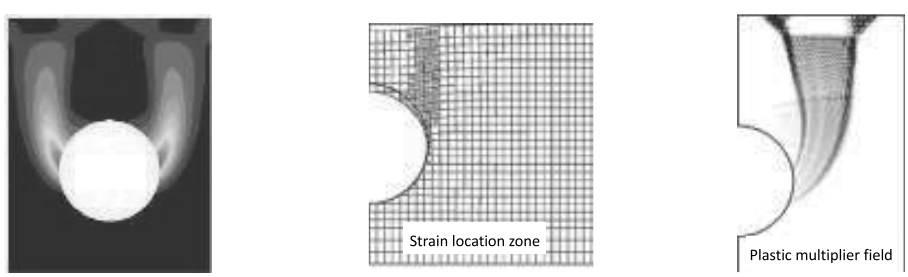

(a) Shear-strain increment (b) Sterpi & Cividini, 2004 (c) Yamamoto et al., 2011

Fig. 9. Shallow tunnel collapse mechanisms.

Equation (25) is changed into $y_0 = r - \sqrt{r^2 - x_0^2}$, and then the analytical results represent the point C below hance. The curved sliding surface (n=2) is applied to analyze the location of point C. The influence of C location on results is shown in Table 3. The sliding surface appears where safety factor is the minimum value. Hence, it shows that point C appears beyond hance when the tunnel depth is less than 6 m. On the contrary, point C appears below hance when the tunnel depth is more than 6 m. Point C is very close to hance when tunnel depth is 6 m. It verifies that x_0 is very close to 6 m (y_0 is close to zero) in Table 1 and Table 2. Therefore, the locations of point C beyond and below hance should be taken into account and the curved sliding surface with n=2 is a reasonable and applicable choice to analyze shallow tunnel collapse mechanisms to save time and to ensure accuracy.

Table 3. The influence of C location on results.

tunnel depth /m		10	8	6	4	2
C below hance	k_{sc}	0.843	0.843	0.894	0.974	1.118
	y_0 /m	-1.165	-0.772	-0.260	-0.031	-0.035
C beyond hance	k_{sc}	0.845	0.845	0.894	0.972	1.102
	y_0 /m	0.011	0.011	0.011	0.451	1.520

Parameter analysis

There are many parameters that influence the shallow tunnel safety factor and the sliding surface distribution. It is meaningful to determine which of these parameters have an obvious influence on tunnel stability.

Given the condition that $F_h=F_0$, $F_v=0$ and locations of point C beyond and below hance are taken into account, the analytical method with curved sliding surface with n=2 is applied to analyze the influence on shallow tunnel collapse mechanisms. The safety factors vary greatly with the time in Figure 7 and this shows that the stresses on sliding surface change greatly during an earthquake. To demonstrate the extent of the stress variation at a sliding surface, the reciprocal of the safety factor is defined as the stress coefficient. When the stress coefficient equals 1, the shear stress is equal to the strength of the ground on the sliding surface. In an earthquake excitation, the safety factor achieves a minimum value when the stress coefficient is a maximum value with $k_h = k_{h0}$ and $k_v = k_{v0}$. Conversely, the safety factor is a maximum value and the stress coefficient is a minimum value with $k_h = -k_{h0}$ and $k_v = -k_{v0}$. The stress coefficient range is defined as the region from the maximum to minimum stress coefficients and it is employed to evaluate the extent of the stress variation on the sliding surface.

(1) Influence of tunnel radius. A shallow tunnel is excavated in the ground where γ=20 kN/m^3, α=35°, c=150 kPa, q'=50 kPa, q=20 kPa, $k_{h0} = k_{v0} = 0.3$, $f_a = 1.3$, r=6 m, h_l=6 m, H=18 m, $\nu = 0.3$ and F_0=218 kN. All the parameters are fixed except the tunnel radius, and then the influence of tunnel radius on shallow tunnels is shown in Figure 10, where $a = k_v = k_h$, the direction of horizontal acceleration with a=0.3 is contrary to with a=-0.3. Tunnel safety factors increase quickly when the tunnel radius decreases from 8 m to 2 m. The tunnel's minimum safety factor increases from 0.73 to 1.70 and the maximum and minimum stress coefficients are reduced from 1.37 and 0.47 to 0.60 and 0.23, respectively, x_0 are below and close to their hances and x_1 decrease from 12.38 m to 6.70 m. The sliding surfaces have a trend to move to vault when the horizontal and vertical acceleration coefficients decrease from 0.3 to 0. The tunnel radius has a significant influence on the shallow tunnel's stability and the sliding surface distribution. Reducing the tunnel radius is a good method to enhance the tunnel's stability and to decrease the stress coefficient range.

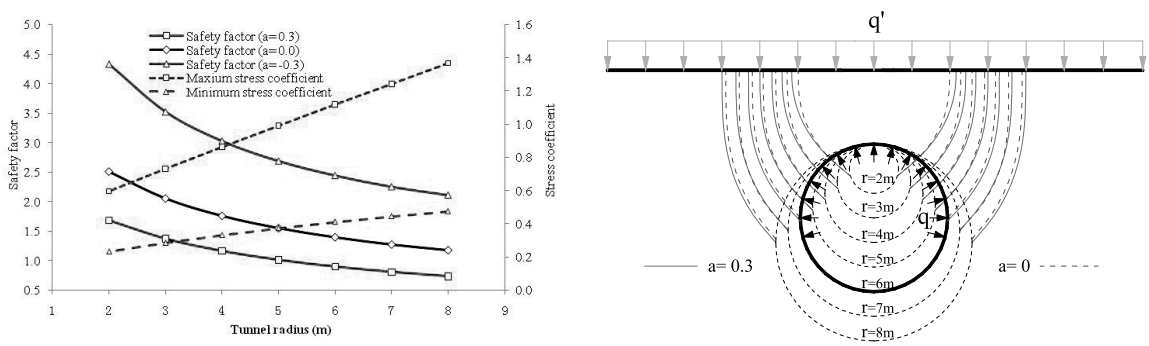

(a) Safety factor on a sliding surface (b) Sliding surface distribution

Fig. 10. Influence of tunnel radius on shallow tunnels in one earthquake excitation.

(2) Influence of tunnel depth. When the tunnel depth serves as a variable, the influence of tunnel depth on shallow tunnels is shown in Figure 11. The tunnel depth has an obvious influence on the tunnel safety factor and the sliding surface distribution. When the tunnel depth decreases from 14 m to 2 m, y_0 increases from -1.77 m to 1.52 m, x_1 decreases from 13.66 m to 8.87 m with a = 0.3, the sliding surface shows a trend of moving to the tunnel vault, and the tunnel minimum safety factor increases from 0.74 to 1.10. The sliding surface with a=0 is obviously different from the sliding surface with a=0.3 when tunnel depth is 2m. But they are close to each other when tunnel depth is 14m. The shallower a tunnel is, the greater the influence of acceleration coefficients on sliding surface is.

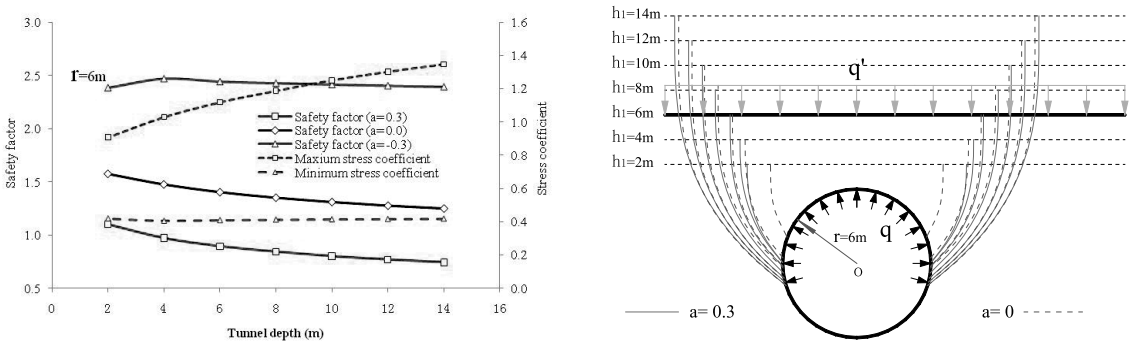

(a) Safety factor on a sliding surface (b) Sliding surface distribution

Fig. 11. Influence of tunnel depth on shallow tunnels in one earthquake excitation.

(3) Influence of amplification factor. The amplification factor serves as a variable, and its influence on shallow tunnels is shown in Figure 12. When the amplification factor increases from 1 to 1.6, the tunnel minimum safety factor decreases from 0.97 to 0.83, the minimum stress coefficient decreases from 0.46 to 0.37, and the maximum stress coefficient increases from 1.03 to 1.21. There is an unobvious influence on the sliding surface distribution. Therefore, the increasing of amplification factor reduces the tunnel safety factor and enlarges the stress coefficient range. Reducing the amplification factor is advantageous to tunnel stability.

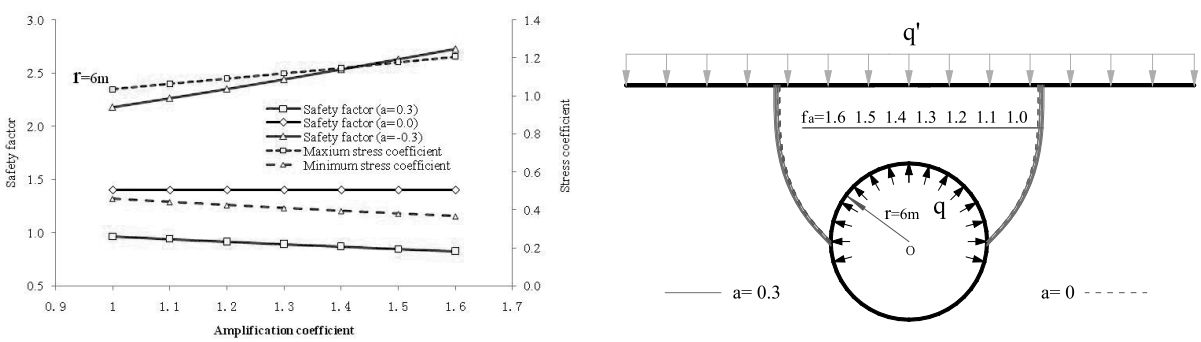

(a) Amplification factor's influence on stability (b) Sliding surface distribution

Fig. 12. Influence of amplification factor on shallow tunnels in one earthquake excitation.

(4) Influence of surface load. The influence of surface load on shallow tunnels is shown in Figure 13. When the surface load q' increases from 10 kPa to 70 kPa, the tunnel minimum safety factor decreases from 0.96 to 0.86, the maximum and minimum stress coefficients increase from 1.04 and 0.31 to 1.16 and 0.46, respectively, and x_1 changes from 10.64 m to 10.00 m with $k_h = k_v = 0.3$. It is clear that the surface load is disadvantageous to tunnel stability and that the surface load has a slight influence on the stress coefficient range and sliding surface distribution.

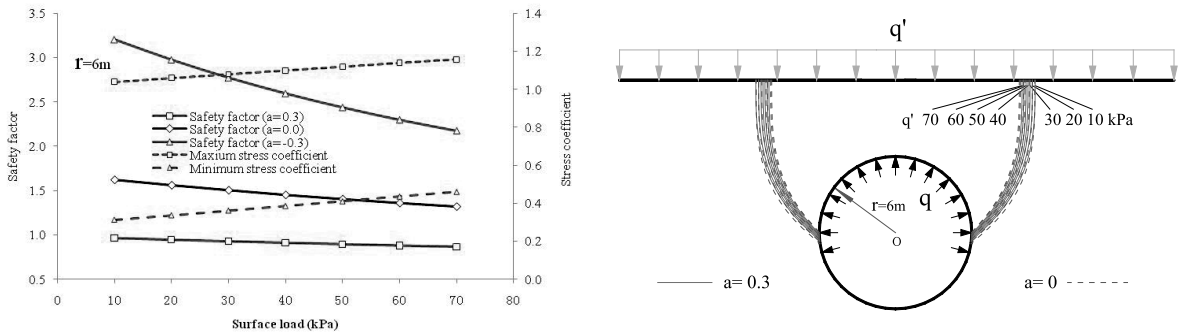

(a) Safety factor on a sliding surface (b) Sliding surface distribution

Fig. 13. Influence of surface load on shallow tunnels in one earthquake excitation.

(5) Influence of supporting pressure. The influence of supporting pressure on shallow tunnels is shown in Figure 14. When the supporting pressure increases from 10 kPa to 70 kPa, the tunnel minimum safety factor increases from 0.88 to 0.98, the maximum and minimum stress coefficients decrease from 1.14 and 0.43 to 1.03 and 0.32, respectively, and x_1 changes from 9.90 m to 10.91 m with a = 0.3. The supporting pressure is advantageous to the tunnel stability and has a slight influence on the stress coefficient range and sliding surface distribution.

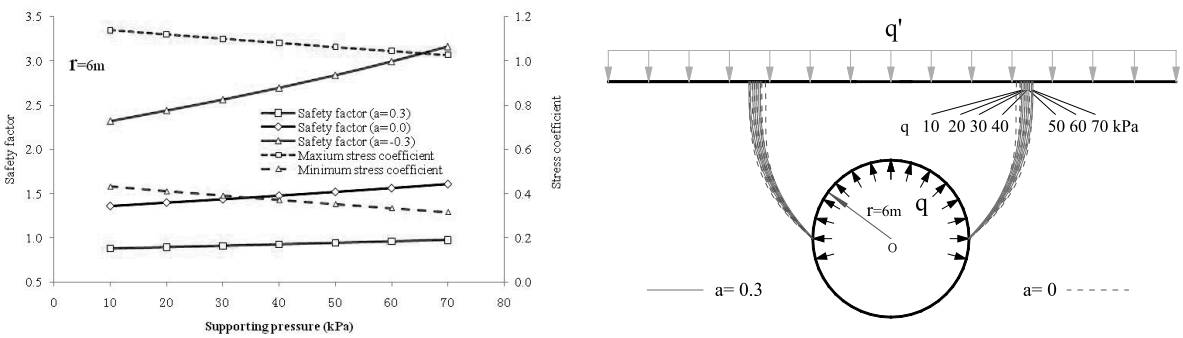

(a) Safety factor on a sliding surface (b) Sliding surface distribution

Fig. 14. Influence of supporting pressure on shallow tunnels in one earthquake excitation.

(6) Influence of friction angle. The influence of friction angle on shallow tunnels is shown in Figure 15. When the surrounding rock's friction angle increases from 5° to 35°, the tunnel minimum safety factor increases from 0.79 to 0.89, the maximum and minimum stress coefficients decrease from 1.27 and 0.53 to 1.12 and 0.41, respectively, y_0 increases from -0.61 m to 0.25m, and x_1 changes from 13.43 m to 10.15 m with a = 0.3. It is doubtless that the friction angle is helpful with respect to tunnel stability and has an obvious influence on the sliding surface distribution and a slight influence on the stress coefficient range.

(7) Cohesion's influence. The influence of cohesion on shallow tunnels is shown in Figure 16. When the surrounding rock's cohesion increases from 25 kPa to 175 kPa the minimum safety factor increases from 0.15 to 1.03, the maximum and minimum stress coefficients decrease from 6.61 and 1.11 to 0.97 and 0.36, respectively, x_0 is close to tunnel radius, and x_1 changes from 7.72 m to 10.40 m with a = 0.3. It is clear that the cohesion has an obvious influence on the tunnel's stability, stress coefficient range, and sliding surface distribution.

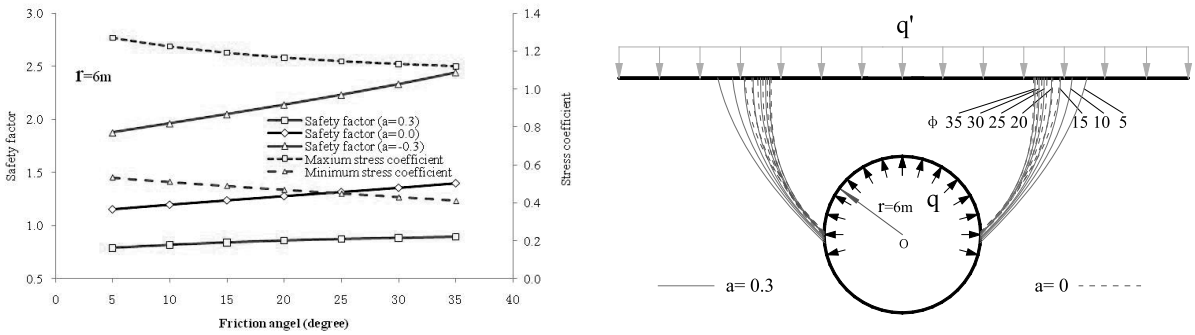

(a) Safety factor on a sliding surface (b) Sliding surface distribution

Fig. 15. Influence of friction angle on shallow tunnels in one earthquake excitation.

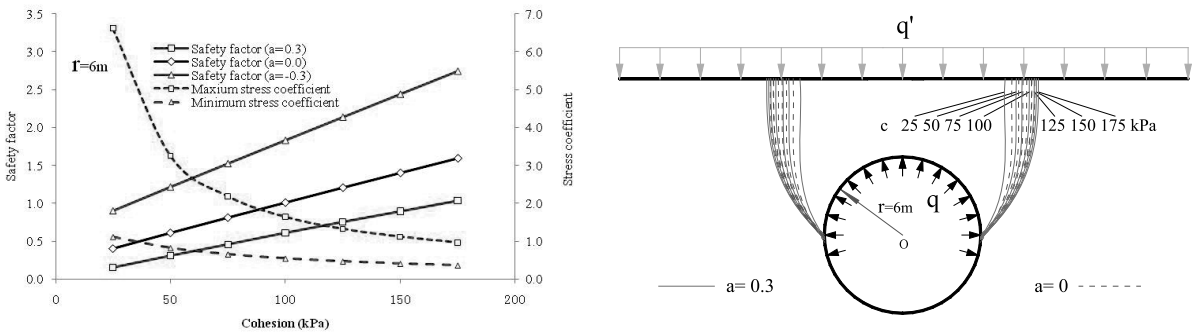

(a) Safety factor on a sliding surface (b) Sliding surface distribution

Fig. 16. Influence of cohesion on shallow tunnels in one earthquake excitation.

The results show that the tunnel radius, friction angle, and cohesion's influence on the shallow tunnel stability was very obvious, so their influence will be analyzed in detail. The parameters in the previous example of this section are used. When the friction angle and cohesion serve as variables, their influences on shallow tunnels' safety factor are shown in table 4 and Figure 17. When the friction angle increases from 5° to 35°, the maximum and minimum increasing values of the safety factors are 0.134 and 0.027, respectively. When the cohesion increases from 50 kPa to 200 kPa the maximum and minimum increasing values of safety factors are 0.866 and 0.759. It is clear that the cohesion's influence on the shallow tunnel stability is greater than the friction angle's influence.

Table 4. Friction angle and cohesion's influence on shallow tunnels' safety factor.

c/kPa		50	75	100	125	150	175	200
	5	0.280	0.408	0.536	0.662	0.788	0.914	1.039
	10	0.293	0.428	0.560	0.689	0.817	0.944	1.071
	15	0.301	0.440	0.576	0.709	0.840	0.970	1.098
φ/°	20	0.306	0.448	0.588	0.724	0.858	0.991	1.121
	25	0.305	0.457	0.596	0.736	0.873	1.008	1.141
	30	0.307	0.457	0.604	0.743	0.884	1.022	1.158
	35	0.307	0.458	0.609	0.752	0.894	1.034	1.173

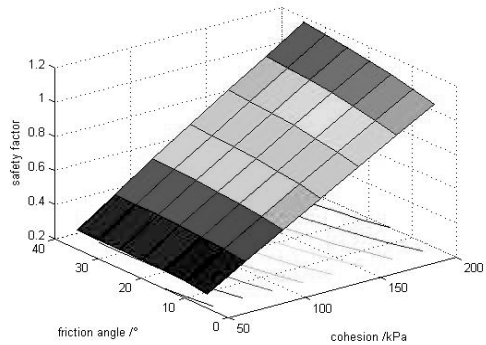

Fig.17. Influence of the friction angle and cohesion on shallow tunnels' safety factor.

The tunnel radius and the cohesion's influences on shallow tunnels' safety factor are shown in table 5 and figure 18. When the tunnel radius decreases from 8 m to 2 m, the maximum and minimum increasing values of the safety factor are 1.167 and 0.490, respectively. When the cohesion increases from 50 kPa to 200 kPa, the maximum and minimum increasing values of the safety factor are 1.421 and 0.743. In a word, the tunnel radius and cohesion's influence on tunnel stability is significant and reducing the tunnel radius and enhancing the cohesion are the most effective ways to increase a tunnel's safety stability.

Table 5. Tunnel radius and cohesion's influence on shallow tunnels' safety factor.

r/m		8	7	6	5	4	3	2
	50	0.225	0.262	0.307	0.366	0.443	0.551	0.715
	75	0.355	0.401	0.458	0.539	0.633	0.769	0.967
	100	0.490	0.542	0.608	0.699	0.810	0.970	1.210
c/kPa	125	0.612	0.674	0.754	0.853	0.986	1.171	1.447
	150	0.731	0.805	0.894	1.010	1.160	1.368	1.679
	175	0.850	0.932	1.034	1.162	1.330	1.562	1.909
	200	0.969	1.060	1.173	1.314	1.499	1.753	2.136

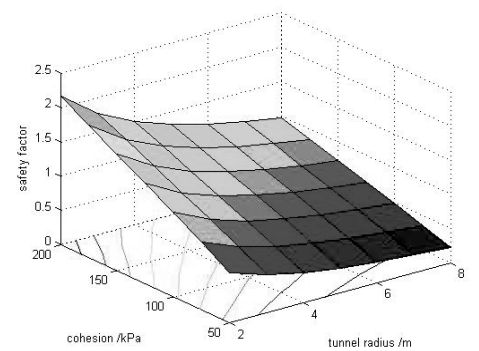

Fig.18. Influences of the tunnel radius and cohesion on shallow tunnels' safety factor.

CONCLUSIONS

The seismic solutions for shallow tunnel collapse mechanisms are presented based on the horizontal slice method and variational principle. The finite difference method was applied for comparison with the analytical results, and then the following conclusions are clear.

It is reasonable and conservative to leave out the vertical force and to assume that the integral of the earth pressure at rest is the horizontal force at vault section AB. The safety factors on a sliding surface change greatly over one earthquake excitation and the cyclic loading should be taken into account when evaluating tunnel stability.

The seismic analysis with the linear sliding surface will overestimate the tunnel stability. The curved sliding surface with 2 undetermined constants, taking into account the different locations of start point, is a reasonable and applicable choice to analyze the shallow tunnel collapse mechanisms to save time while ensuring accuracy. The analytical results are in good agreement with the numerical simulation and previous studies.

Parameter analysis using analytical method shows that the tunnel depth and radius, the surrounding rock's friction angle, and the cohesion have an obvious influence on the sliding surface distribution. The tunnel radius and the surrounding soil cohesion are the two most important factors influencing tunnel stability. Reducing the tunnel radius and increasing cohesion are very useful ways to enhance tunnel stability.

ACKNOWLEDGMENT

This work was supported by the National Science Foundation of China (50334060, 41672304, and 51708373) and the Sichuan Province Education Department's Scientific Research Foundation of China (11ZB055 and 16TD0006).

REFERENCES

Amorosi, A & Boldini, D. 2009. Numerical modelling of the transverse dynamic behaviour of circular tunnels in clayey soils. *Soil Dynamics and Earthquake Engineering,* **29**(6): 1059-1072.

Argyroudis, SA & Pitilakis, KD. 2012. Seismic fragility curves of shallow tunnels in alluvial deposits. *Soil Dynamics and Earthquake Engineering,* **35**: 1-12.

Azadi, M & Mir Mohammad Hosseini, SM. 2010. Analyses of the effect of seismic behavior of shallow tunnels in liquefiable grounds. *Tunnelling and Underground Space Technology,* **25**(5): 543-552.

Bilotta, E., Lanzano, G., Russo, G., Santucci de M, F., Aiello, V., Conte, E., Silvestri, F. & Valentino, M. 2007. *Pseudostatic and dynamic analyses of tunnels in transversal and longitudinal directions.* Paper presented at the Proceedings of the 4th international conference on Earthquake Geotechnical Engineering.

Chen, J., Jiang, L., Li, J. & Shi, X.. 2012. Numerical simulation of shaking table test on utility tunnel under non-uniform earthquake excitation. *Tunnelling and Underground Space Technology,* **30**: 205-216.

Chen, Z.Y. & Shen, H. 2014. Dynamic centrifuge tests on isolation mechanism of tunnels subjected to seismic shaking. *Tunnelling and Underground Space Technology,* **42**: 67-77.

Davis, EH, Gunn, MJ, Mair, RJ & Seneviratine, HN. 1980. The stability of shallow tunnels and underground openings in cohesive material. *Geotechnique,* **30**(4): 397-416.

Fraldi, M & Guarracino, F. 2009. Limit analysis of collapse mechanisms in cavities and tunnels according to the Hoek–Brown failure criterion. *International Journal of Rock Mechanics and Mining Sciences,* **46**(4): 665-673.

Ghosh, S. 2010. Pseudo-dynamic active force and pressure behind battered retaining wall supporting inclined backfill. *Soil Dynamics and Earthquake Engineering,* **30**(11): 1226-1232.

Gomes, R.C., Gouveia, F., Torcato, D. & Santos, J. 2015. Seismic response of shallow circular tunnels in two-layered ground. *Soil Dynamics and Earthquake Engineering,* **75**: 37-43.

Huang, F & Yang, XL. 2011. Upper bound limit analysis of collapse shape for circular tunnel subjected to pore pressure based on the Hoek–Brown failure criterion. *Tunnelling and Underground Space Technology,* **26**(5): 614-618.

Huang, F., Zhang, D., Sun, Z. & Jin, Q. 2012. Upper bound solutions of stability factor of shallow tunnels in saturated soil based on strength reduction technique. *Journal of Central South University,* **19**: 2008-2015.

Jaky, J. 1944. The coefficient of earth pressure at rest. *Journal of the Society of Hungarian Architects and Engineers,* **78**(22): 355-358.

Kolathayar, S. & Ghosh, P. 2009. Seismic active earth pressure on walls with bilinear backface using pseudo-dynamic approach. *Computers and Geotechnics,* **36**(7): 1229-1236.

Lei, M., Peng, L. & Shi, C.. 2014. Calculation of the surrounding rock pressure on a shallow buried tunnel using linear and nonlinear failure criteria. *Automation in Construction,* **37**: 191-195.

Lei, M., Peng, L. & Shi, C.. 2015. Model test to investigate the failure mechanisms and lining stress characteristics of shallow buried tunnels under unsymmetrical loading. *Tunnelling and Underground Space Technology,* **46**: 64-75.

Munwar Basha, B. & Sivakumar Babu, G.L. 2010. Reliability assessment of internal stability of reinforced soil structures: A pseudo-dynamic approach. *Soil Dynamics and Earthquake Engineering,* **30**(5): 336-353.

Pitilakis, K., Tsinidis, G., Leanza, A. & Maugeri, M.. 2014. Seismic behaviour of circular tunnels accounting for above ground structures interaction effects. *Soil Dynamics and Earthquake Engineering,* **67**: 1-15.

Saada, Z, Maghous, S & Garnier, D. 2013. Pseudo-static analysis of tunnel face stability using the generalized Hoek–Brown strength criterion. *International Journal for Numerical and Analytical Methods in Geomechanics,* **37**(18): 3194-3212.

Sahoo, J.P. & Kumar, J. 2014. Stability of a circular tunnel in presence of pseudostatic seismic body forces. *Tunnelling and Underground Space Technology,* **42**: 264-276.

Steedman, R.S. & Zeng, X. 1990. The influence of phase on the calculation of pseudo-static earth pressure on a retaining wall. *Geotechnique,* **40**(1): 103-112.

Sterpi, D & Cividini, A. 2004. A physical and numerical investigation on the stability of shallow tunnels in strain softening media. *Rock Mechanics and Rock Engineering,* **37**(4): 277-298.

Tao, L., Hou, S., Zhao, X., Qiu, W., Li, T., Liu, C. & Wang, K.. 2015. 3-D shell analysis of structure in portal section of mountain tunnel under seismic SH wave action. *Tunnelling and Underground Space Technology,* **46**: 116-124.

Wang, W.L., Wang, T.T., Su, J.J., Lin, C.H., Seng, C.R. & Huang, T.H. 2001. Assessment of damage in mountain tunnels due to the Taiwan Chi-Chi Earthquake. Tunnelling and underground space technology, **16**(3), 133-150.

Wang, ZZ & Zhang, Z. 2013. Seismic damage classification and risk assessment of mountain tunnels with a validation for the 2008 Wenchuan earthquake. Soil Dynamics and Earthquake Engineering, **45**: 45-55.

Yamamoto, K., Lyamin, A.V., Wilson, D.W., Sloan, S.W. & Abbo, A.J. 2011. Stability of a circular tunnel in cohesive-frictional soil subjected to surcharge loading. Computers and Geotechnics, **38**(4), 504-514.

Yang, X. & Huang, F. 2009. Stability analysis of shallow tunnels subjected to seepage with strength reduction theory. Journal of Central South University of Technology, **16**: 1001-1005.

Yi, C.P., Lu, W.b, Zhang, P., Johansson, D. & Nyberg, U. 2016. Effect of imperfect interface on the dynamic response of a circular lined tunnel impacted by plane P-waves. Tunnelling and Underground Space Technology, **51**: 68-74.

Submitted: 05/06/2017
Revised: 04/01/2018
Accepted: 28/05/2018

التحليل الزلزالي لآليات انهيار الأنفاق الضحلة باستخدام طريقة الشريحة الأفقية

قوه زي هونغ، **ليو شين رونغ، *لي لين وتشو تشانيوان**
*كلية الهندسة المدنية، جامعة سيتشوان الزراعية، دوجيانغيان، الصين
**كلية الهندسة المدنية، جامعة تشونغتشينغ، الصين
***المعهد العالي لمركز البحوث الهندسية للوقاية من الكوارث والحد منها في المناطق الريفية بستشوان، دوجيانغيان، الصين

الخلاصة

يقدم هذا البحث طريقة تحليلية لتقييم آليات انهيار الأنفاق أثناء الزلازل، وقد تم عمل حلول زلزالية اعتماداً على طريقة الشريحة الأفقية ومبدأ التباين. تم استخدام أسطح منزلقة ومختلفة لمقارنتها مع بعضها البعض وتم استخدام طريقة الفروق المنتهية للتحقق من النتائج التحليلية. واتضح من النتائج أنه من الضروري ترك القوة العمودية واعتبار ضغط الأرض الثابت بمثابة الضغط الأفقي في القبو. الأسطح المنزلقة المنحنية أكثر موضوعية من السطح المنزلق الخطي. تتغير عوامل الأمان في الأنفاق على سطح منزلق بين 0.89 و2.44 أثناء الزلازل بمعدل 0.3 جرام. عندما يكون عدد الثوابت غير المحددة 2 ومع أخذ المواقع المختلفة لنقطة بداية الضرر في الاعتبار، يكون السطح المنزلق المنحني مناسباً لتحليل آليات انهيار الأنفاق الضحلة، وتتفق النتائج التحليلية بشكل ممتاز مع المحاكاة الرقمية والدراسات السابقة. أظهر تحليل المعلمات أن عمق النفق ونصف القطر وزاوية الاحتكاك وتماسك التربة لهم تأثير واضح على توزيع السطح المنزلق. ويعد نصف قطر النفق وتماسك التربة المحيطة من أهم العوامل المؤثرة في استقرار النفق، حيث أن تقليل نصف قطر النفق وزيادة التماسك من أكثر الطرق المفيدة لتعزيز استقرار النفق الضحل أثناء الزلازل.